Predicting non-equilibrium patterns beyond thermodynamic concepts: application to radiation induced microstructures.

Laurence Luneville, Philippe Garcia, David Simeone

Predicting Nonequilibrium Patterns beyond Thermodynamic Concepts: Application to Radiation-Induced Microstructures

L. Luneville
CEA, DES, ISAS, DM2S, Paris-Saclay F-91191 Gif-sur-Yvette, France

P. Garcia
CEA, DES, IRESNE, DEC, Cadarache F-13108 Saint-Paul-Lez-Durance, France

D. Simeone[*]
CEA, DES, ISAS, DMN, Paris-Saclay F-91191 Gif-sur-Yvette, France

In this work, we derive an analytical model to predict the appearance of all possible radiation-induced steady states and their associated microstructures in immiscible $A_{\bar{c}}B_{1-\bar{c}}$ alloys, an example of a nonequilibrium dynamical system. This model is assessed against numerical simulations and experimental results which show that different microstructures characterized by the patterning of A-rich precipitates can emerge under irradiation. We demonstrate that the steady-state microstructure is governed by irradiation conditions and also by the average initial concentration of the alloy $\bar{c}$. Such a dependence offers new leverage for tailoring materials with specific microstructures overcoming limitations imposed by the equilibrium thermodynamic phase diagram.

Although the features of equilibrium phenomena have been extensively studied in the past, physical systems in nature exist in nonequilibrium states [1–4]. Their study is of substantial interest to basic science and also has promising technological applications. In contrast to phase transitions at thermal equilibrium, transitions out of equilibrium are far less understood as they lack a comprehensive underlying theory [3,5,6]. Understanding the appearance of microstructural patterns is a burning issue in nanotechnology where materials are processed far from equilibrium [7]. Predicting all possible nonequilibrium steady states and rationalizing conditions in which they appear constitute substantial challenges. Beyond the academic interest, modeling out-of-equilibrium microstructures can inspire new methods for manufacturing materials with tailored properties [3], such as is sought in ion beam processing of optoelectronics materials [7] or in certain nuclear applications [8,9].

In the absence of radiation, the kinetics of phase separation in immiscible AB alloys is dictated by the Landau-Ginzburg equation, also known as model B in the Halperin-Hohenberg classification [10] or as the Cahn-Hilliard equation in metallurgy [3]. The composition of A-rich precipitates resulting from this phase separation is given by the thermodynamic equilibrium phase diagram. Under irradiation, however, as impinging particles (neutrons, ions, etc.) slow down, they eject atoms originally at rest in the crystal which leads to temperature independent mixing of atoms known as ballistic mixing, and which is insensitive to the nature of chemical bonds between atoms [11,12]. This external dynamics, which depends on the irradiation flux ϕ and the nature of the particle beam, "drives" the system away from its thermodynamic equilibrium [13]. Although steady states are eventually reached, the chemical composition of radiation-induced A-rich precipitates reaches values at large timescales which one cannot predict from the study of the thermodynamic equilibrium phase diagram [14,15].

Attempts [16–18] have been made in the past to compute the chemical composition of A-rich precipitates occurring under irradiation and have given rise to a theory known as the theory for driven alloys [16]. In this approach, a kinetic enhancement factor $[D^{\mathrm{ball}}(\phi)]/[D^{\mathrm{therm}}(T,\phi)]$ characterizes the competition between ballistic mixing induced by irradiation, associated with the temperature independent diffusion coefficient $D^{\mathrm{ball}}(\phi)$ and thermally activated diffusion enhanced by the irradiation flux ϕ and characterized by the diffusion coefficient $D^{\mathrm{therm}}(T,\phi)$. This leads to a "law of corresponding states" in which the chemical composition of precipitates under irradiation is the same as that given by the equilibrium thermodynamic phase diagram at an "effective" temperature defined by $T_{\mathrm{eff}} = T\{1 + [D^{\mathrm{ball}}(\phi)/D^{\mathrm{therm}}(T,\phi)]\}$ [16]. The theory qualitatively explains the existence of a solid solution at low temperature under irradiation [16] but fails to describe radiation-induced patterning of A-rich precipitates observed in Monte Carlo simulation studies [19,20].

To overcome this shortcoming, the mechanism of ballistic mixing needs to be described in greater detail [11]. It can be modeled as a random-walk process within the continuum approximation [21,22], which induces a rate of change of the local composition $[\partial c(\mathbf{r}, t)]/\partial t$ proportional to $\int p_R(\mathbf{r}, \mathbf{r}')c(\mathbf{r}', t)d\mathbf{r}' - c(\mathbf{r}, t)$, where the probability density function $p_R(\mathbf{r}, \mathbf{r}')$ represents the ability of ejecting an atom located at $\mathbf{r}$ at a distance $|\mathbf{r} - \mathbf{r}'|$; R defines the "interaction range" for ballistic mixing and the last term $c(\mathbf{r}, t)$ is introduced to satisfy the constraint of mass conservation. Molecular dynamics simulations have shown that $p_R(\mathbf{r}, \mathbf{r}') = p_R(|\mathbf{r} - \mathbf{r}'|) \propto \exp(-|\mathbf{r} - \mathbf{r}'|/R)$ [13,23]. By analogy with microphase separation observed in diblock copolymers [24], we have modeled the dynamics of ballistic mixing by adding the following nonlocal pairwise interaction term to the free energy [11,13]:

$$\mathcal{G}[\theta] = \frac{1}{2} \int \int \theta(\mathbf{r})g_R(|\mathbf{r} - \mathbf{r}'|)\theta(\mathbf{r}')d\mathbf{r}d\mathbf{r}'. \quad (1)$$

In Eq. (1), all variables are dimensionless [25]. $\theta(\mathbf{r})$ is a scalar order parameter (OP) (in reduced units) proportional to the local concentration of species A in the alloy [13,25]. $g_R(|\mathbf{r} - \mathbf{r}'|)$ characterizes the nonlocal interaction associated with ballistic mixing and it is related to $p_R(|\mathbf{r} - \mathbf{r}'|)$ via the following relationship: $-\nabla^2 g_R(x) = \delta(x) - p_R(x)$ [12,13,18]. When $R \rightarrow 0$, as is the case for an electron irradiation, the theory of driven alloys is recovered and $D^{\mathrm{ball}}(\phi)$ is shown to be proportional to the second moment of $p_R(x)$ [18]. When $R \rightarrow \infty$, $g_R(x)$ is identical to the Coulomb-like kernel describing block copolymer phase separation [24]. The distinction between the spatial patterns occurring under irradiation and in diblock copolymers lies in the existence of a finite value of R which scales the range of the interaction. In that sense, our approach constitutes an attempt to unify under a single theory the solution to both problems.

The evolution of $\theta(\mathbf{r}, t)$ is governed by the following Eq. [13]:

$$\frac{\partial \theta(\mathbf{r}, t)}{\partial t} = \nabla^2 \frac{\delta \mathcal{L}[\theta]}{\delta \theta(\mathbf{r}, t)}, \quad (2)$$

with boundary and initial conditions provided, respectively, by $\nabla \theta(\mathbf{r}, t) = 0$ at the domain boundary and $\theta(\mathbf{r}, 0) = \bar{\theta}$. Since two dynamics are acting upon the system independently of each other, the Lyapounov $\mathcal{L}[\theta]$ functional in Eq. (2) may further be expressed as the sum of these two competing contributions, one which is purely thermodynamic in nature and the other which is due to radiation related processes [11,18,25]:

$$\mathcal{L}[\theta] = \mathbf{F}[\theta] + \Delta(T, \phi)\mathcal{G}[\theta]. \quad (3)$$

The free energy $\mathbf{F}[\theta]$ reflects the property of an immiscible AB alloy to decompose in the absence of irradiation. It may phenomenologically be written in the weak segregation regime as a Ginzburg-Landau expansion in $\theta(\mathbf{r})$ and $\nabla \theta(\mathbf{r})$ as $F_0[\theta] + \frac{1}{2} \int |\nabla \theta(\mathbf{r})|^2$. $F_0[\theta]$ captures the bulk contribution and assumes the form of a (Landau) expansion in $\theta(\mathbf{r})$. It is written as [25]

$$F_0[\theta] = \int \left(\frac{\theta(\mathbf{r})^4}{4} - \frac{\theta(\mathbf{r})^2}{2} \right) d\mathbf{r}. \quad (4)$$

The second term (Ginzburg) in $\mathbf{F}[\theta]$ represents the energy cost associated with a local variation of $\theta(\mathbf{r})$. $\Delta(T, \phi)$ is proportional to the ratio of the athermal diffusion coefficient which characterizes ballistic mixing over the radiation-enhanced mobility $[D^{\mathrm{therm}}(T, \phi)]/k_BT$ (k_B is the Boltzmann constant). The value of $\Delta(T, \phi)$ determines the relative importance of athermal effects *vis-à-vis* thermally induced phenomena, all of which are radiation related. In this work, we assume that the radiation-enhanced mobility is independent of the concentration $c(\mathbf{r}, t)$ or, in other words, that $\Delta(T, \phi)$ is independent of the reduced OP $\theta(\mathbf{r})$, and restrict the analysis to the weak segregation regime, which means $F_0[\theta]$ is given by the Landau expansion [Eq. (4)]. We have chosen to apply these simplifying assumptions in order to be capable of formulating analytical solutions to the problem which reveal more straightforwardly how and which physical quantities determine stable microstructures under irradiation. This does not affect the scope of our work, as the first restriction could be lifted by adopting the so-called degenerate-mobility approach [26] and the second could similarly be lifted by using the logarithmic free-energy model as an alternative to the Landau expansion in the strong segregation regime [3]. However, this necessarily requires minimizing $\mathcal{L}[\theta]$ numerically.

The competition between thermodynamic and external forces acting in parallel leads to the emergence of different steady states depending on the values of external parameters ϕ and T, i.e., $\Delta(T, \phi)$ and R, which characterizes the nature of the particle beam. To illustrate this point, Fig. 1 shows the concentration distribution of species A at infinite time $c(\mathbf{r}, \infty)$ obtained from a numerical resolution of Eq. (2) in an irradiated immiscible $A_{\bar{c}}B_{1-\bar{c}}$ alloy subjected to a constant flux ϕ of 1 MeV krypton ions and maintained at constant temperature T. Different periodic patterns associated with zero-, one-, two-, or three-dimensional composition modulations [SS, S, C, and B in Figs. 1(g), 1(a), 1(c), and 1(e), respectively] emerge. It stands to reason that irradiation conditions (temperature, nature, and flux of particle beam) influence the resulting steady-state microstructure. What this simulation shows, however, is that the different steady-state composition modulations are also dependent upon the average composition of the alloy. Figure 1 further illustrates that these basic modulations may combine to create complex patterns [see Figs. 1(b), 1(d), and 1(f)]. An alternative analytical approach may be used to derive all radiation-induced
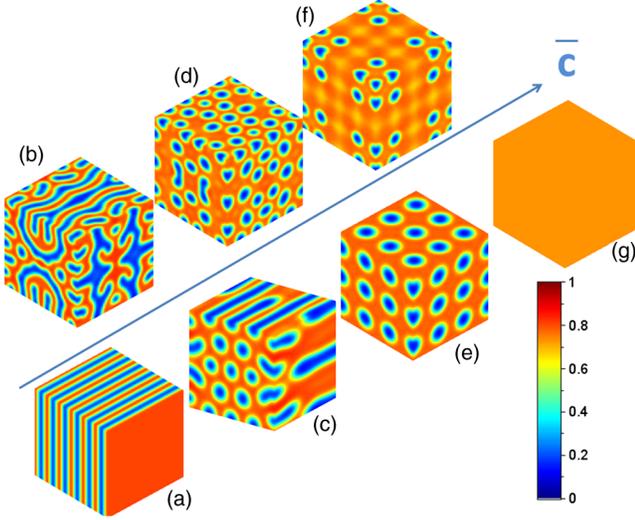
FIG. 1. Ag isoconcentrations resulting from the 3D numerical resolution of Eq. (2) in a $Ag_{\bar{c}}Cu_{1-\bar{c}}$ alloy irradiated with 1 MeV Kr ions at 330 K with a flux of $\phi = 10^{11}$ cm^{-2} s^{-1}. Distinct periodic microstructures emerge depending upon the average Ag concentration $\bar{c}$ [(a) 1D stripes (S), (c) cylinders forming hexagonal patterns (C), (e) 3D body-centered cubic structures ($\bar{c} = 0.65$) (B), (g) solid solution ($\bar{c} = 0.75$) (SS)]. Microstructures associated with the coexistence of such domains are also plotted [(b) $S + C$, (d) $C + B$, (f) $B + SS$].

steady-state microstructures. All possible steady states relative to Eq. (2) are obtained from the minimization of $\mathcal{L}[\theta]$ under the constraint of mass conservation [$\bar{\theta} = (1/V) \int \theta(\mathbf{r}, t) \mathbf{dr}$]. As the fourth order term $\theta(\mathbf{r}, t)^4/4$ in Eq. (4) damps the amplitude of the OP but does not change its modulation, information on the spatial modulations of $\theta(\mathbf{r})$ is contained in the quadratic part of $\mathcal{L}[\theta]$ [13] only. In Fourier space, this term reduces to $\int [D(q)/2] |\hat{\theta}(q, t)|^2 d\mathbf{q}$ and $D(q)$ is given by

$$D(q) = -1 + q^2 + \Delta(T, \phi) \hat{g}_R(q), \qquad (5)$$

where $\hat{g}_R(q) = [R^2(2 + q^2 R^2)/(1 + q^2 R^2)^2]$ is the Fourier transform of $g_R(r)$.

The spatial modulations of steady states are therefore obtained by determining the values of q noted $q_0(R, \Delta(T, \phi))$, that cancel out the first derivative of $D(q)$. Note that the wave vector $q_0(R, \Delta(T, \phi))$ is not only dependent upon the magnitude of the interaction Δ, as is the case for morphological transitions occurring in phase separation of diblock copolymers [24,27], but also on the range of the interaction R related to radiation-induced ballistic mixing.

When solving $D'(q) = 0$ one encounters two distinct situations. Either $q_0(R, \Delta(T, \phi)) = 0$, in which case steady states are nonperiodic. Only macroscopic A-rich precipitates against a B-rich background can be produced. This microstructure is similar to a spinodal decomposition encountered

in the absence of radiation. Furthermore, the minimization of $\mathcal{L}[\theta]$ leads to two distinct values of the solubility limits $A_s = \max(\theta(\mathbf{r}, \infty)) = \pm\sqrt{1 - \Delta(T, \phi)\hat{g}_R(0)}$. The condition $0 \leq \Delta(T, \phi)\hat{g}_R(0) \leq 1$ defines the limit of the spinodal decomposition regime. As A_s is independent of the average concentration $\bar{\theta}$, a law of corresponding states may apply. By comparing the OP under irradiation and in the absence of irradiation, one may derive an expression for the effective temperature which coincides with the effective temperature defined in the theory of driven alloys [16].

In the second situation, $q_0(R, \Delta(T, \phi)) \neq 0$, periodic steady states exhibiting spatial modulations of A-rich precipitates of wavelength $L = [2\pi/q_0(R, \Delta(T, \phi))]$ emerge, leading to a pattern regime. This regime is defined by the two conditions: $q_0(R, \Delta(T, \phi)) > 0$ and $\Delta(T, \phi)\hat{g}_R(0) \geq 1$. This implies that $D(q_0)$ is bounded by upper (0) and lower (-1) values

However, it remains impossible at this stage to determine microstructures associated with these steady states, i.e., the patterning of A-rich precipitates. As only wave vectors in the neighborhood of $q_0(R, \Delta(T, \phi))$ exist at large timescales, $D(q)$ can be approximated by $D(q_0) + [D''(q_0)/8q_0^2](q^2 - q_0^2)$ and $\mathcal{L}[\theta]$ reduces to the Swift-Hohenberg (SH) functional $\mathcal{L}^{SH}[\theta]$, extensively used to describe nonequilibrium patterning in Rayleigh-Bénard convection [4], magnetic thin films [28]. One-, two-, or three-dimensional ground states of the SH functional resulting in modulations referred to as S (stripes), C (cylinders forming hexagonal patterns), and B (spherical particles forming a body-centered cubic structure) are given by the periodic functions $\psi_{q_0}(\mathbf{r})$ [29,30] listed in Table I.

One may now go one step beyond and compute the microstructures in the pattern regime. To do so, one assumes a one-mode approximation:

$$\theta(\mathbf{r}, \infty) = \bar{\theta} + \alpha\psi_{q_0}(\mathbf{r}), \qquad (6)$$

where the scalar quantity α defines the amplitude of the modulation of the reduced steady-state OP. The $\psi_{q_0}(\mathbf{r})$ functions are spatially periodic and have a zero spatial average, thus guaranteeing conservation of mass. Replacing this expression for $\theta(\mathbf{r}, \infty)$ into the expression for $\mathcal{L}[\theta]$ and averaging $\mathcal{L}[\theta]$ over wavelength L, an approximate coarse-grained free-energy density $\mathcal{U}(\alpha, \bar{\theta}) = \langle \mathcal{L}[\theta]\rangle/L^3$ can be

TABLE I. Definition of $\psi_{q_0}(\mathbf{r})$ functions and values of their different spatial averages $M_p = \langle \psi_{q_0}{}^p \rangle$ ($p = 2, 3, 4$).

	ψ_{q_0}	M_2	M_3	M_4
S	$\cos(q_0 x)$	$\frac{1}{2}$	0	$\frac{3}{8}$
C	$\cos(q_0 x)\cos(q_0 y/\sqrt{3}) + \frac{1}{2}\cos(2q_0 y/\sqrt{3})$	$\frac{3}{8}$	$\frac{3}{16}$	$\frac{45}{128}$
B	$\cos(q_0 x)[\cos(q_0 y) + \cos(q_0 z)]$ $+ \cos(q_0 y)\cos(q_0 z)$	$\frac{3}{4}$	$\frac{3}{4}$	$\frac{135}{64}$

analytically computed and now enables us to discuss the emergence of microstructures in the pattern regime:

$$\mathcal{U}(\alpha, \bar{\theta}) = \mathcal{U}_{SS} + [3\bar{\theta}^2 + D(q_0)]\frac{\alpha^2}{2}\langle\psi_{q_0}^2\rangle$$

$$+ \bar{\theta}\alpha^3\langle\psi_{q_0}^3\rangle + \frac{\alpha^4}{4}\langle\psi_{q_0}^4\rangle, \qquad (7)$$

where $\mathcal{U}_{SS} = \bar{\theta}^4/4 - \{\bar{\theta}^2[1 - \Delta(T,\phi)\hat{g}_R(0)]/2\}$ is the averaged free-energy density of the solid solution (SS). As $\mathcal{L}^{SH}[\psi_{q_0}] \geq \mathcal{L}[\psi_{q_0}]$, the Rayleigh-Ritz variational principle ensures that the minimization of $\mathcal{U}(\alpha, \bar{\theta})$ with respect to α is the best approximation for the ground state microstructures of $\mathcal{L}[\theta]$. $\mathcal{U}(\alpha, \bar{\theta})$ exhibits an absolute minimum for certain values of α, noted α_j [$j = (S), (C)$, or B]. Microstructures associated with these values, i.e., for specific composition modulations of A-rich precipitates, can combine to create coexistence domains (upper panels in Fig. 1) computed from a Maxwell-like equal-area construction rule [29]. It is quite obvious from Eq. (7) that each particular value of α_j depends upon irradiation conditions via $D(q_0)$ and also upon the average composition of the alloy $\bar{\theta}$. This analytical approach confirms the dependence of the microstructure upon $\bar{\theta}$ observed in our numerical simulation (see Fig. 1). Such a dependence of microstructures can be understood within the framework of the theory of nonequilibrium dynamic systems [31]. Therefore, the mass conservation implies that the average concentration pushes the nonlinear dynamics describing the formation of A-rich precipitates toward distinct attractors leading to different microstructures in the pattern regime.

Since we have shown that the steady-state microstructures in the pattern regime were dependent upon $D(q_0)$ and $\bar{\theta}$ only, one may define a two-dimensional structure diagram as illustrated in Fig. 2. We have added to this figure the microstructures resulting from the numerical simulation shown in Fig. 1 which coincide perfectly with those of our analytical approach, thus justifying the Rayleigh-Ritz assumption. Note that the solid solution in Fig. 2 appears as a particular microstructure within the pattern regime corresponding to $\alpha_{SS} = 0$. It is not in any way a singular steady state contrary to previous claims [11]. The fundamental point this figure highlights is that in the pattern regime, two alloys with different average compositions $\bar{\theta}$ irradiated under identical temperature T and flux ϕ, i.e., leading to a unique $D(q_0)$ value, may exhibit different microstructures.

The calculation of $\mathcal{U}(\alpha, \bar{\theta})$ enables computing not only all possible microstructures emerging in the pattern regime but also their solubility limits $A_s^j = \max(\theta_j(\mathbf{r}))$. Figure 3(a) represents the comparison between $A_s^j - \bar{\theta}$ extracted from the numerical resolution of Eq. (2) and resulting from the minimization of $\mathcal{U}(\alpha, \bar{\theta})$ as a function of the average composition of the alloy for $D(q_0) = -0.30$. The good
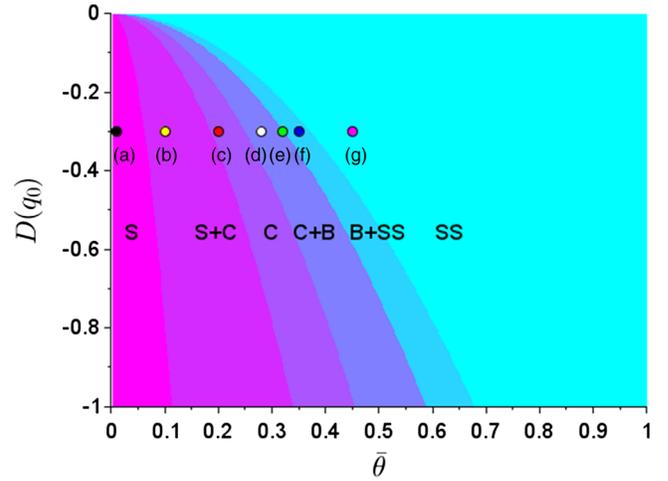
FIG. 2. Theoretical structure diagram displaying all possible radiation-induced microstructures in AgCu. Microstructures presented in Fig. 1 [$D(q_0) = -0.3$] resulting from the numerical resolution of Eq. (2) [$\Delta(T,\phi) = 0.0151$, i.e., $D^{ball}(\phi) = 0.01D^{therm}(T,\phi)$, and $R = 2$] are also plotted (colored dots).

agreement between numerical and analytical solubility limits displayed in Fig. 3(a) further demonstrates the relevance of our analytical approach and, in particular, the use of trial functions $\psi_{q_0}(\mathbf{r})$ to describe microstructures. Figure 3(b) provides a comparison between theoretical values of A_s^C derived from the minimization of $\mathcal{U}(\alpha, \bar{\theta})$ [see Eq. (7)] (blue line) and resulting from measurements (red stars) of x-ray diffraction patterns collected on irradiated $Ag_{0.4}Cu_{0.6}$ samples [32]. The fair agreement between
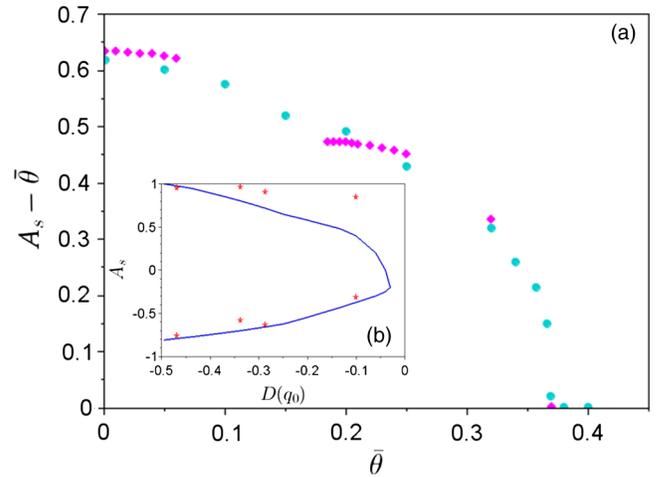
FIG. 3. (a) Values of $A_s^j - \bar{\theta}$ resulting from the minimization of $\mathcal{U}$ in the pattern regime (magenta diamonds) and obtained from the numerical resolution of Eq. (2) (cyan dots) [$D(q_0) = -0.30$]. The absolute value of the relative error between the analytical and numerical A_s values is lower than 5%, justifying the one-mode approximation. (b) Measured (red stars) and analytical (blue line) values of A_s^C plotted as a function of $D(q_0)$ for $\bar{\theta} = -0.2$ in the pattern regime.

analytical and experimental values [Fig. 3(b)] validates our approach. A possible explanation for the observed discrepancy between measured and calculated positive A_s^C values [Fig. 3(b)] may be due to the highly asymmetric shape of Bragg peaks, which in turn leads to inaccurate values of unit cell parameters for Ag-rich precipitates. This will lead to inaccurate values of A_s^C resulting from the application of Vegard's law. Moreover, this model is still essentially a coarse-grained model which overlooks many atomistic aspects of the physical system (point defects, dislocations, grain boundaries, etc). These are definitely present in the experimental setup. So the discrepancy could also be due to limitations of the model.

The characteristics of pattern regimes which Figs. 2 and 3 reveal preclude describing radiation-induced microstructures using the concept of effective temperature. Moreover, our approach succeeds in explaining previously reported experiments [15]: CuCo alloys of different average compositions, irradiated under identical conditions, have been shown to develop different solubility limits.

In summary, this work demonstrates that only two distinct regimes can be produced under irradiation: a spinodal decomposition associated with nonperiodic steady states and a pattern regime associated with a single composition modulation defined by $q_0(T, \phi, R)$. The pattern regime is characterized by distinct microstructures depending not only upon irradiation conditions but also upon the average composition of the alloy $\bar{c}$. To treat the problem comprehensively, an original approach is proposed which enables us to determine all possible microstructures emerging in the pattern regime. This dependence of the microstructure upon $\bar{c}$ provides a new tool for tailoring radiation-induced microstructures, thus overcoming the limitations intrinsic to irradiation conditions.

---

[*]david.simeone@cea.fr

[1] G. Van Kampen, *Stochastic Processes in Physics and Chemistry* (Elsevier, Amsterdam, 1992).

[2] G. Nicolis and I. Prigogine, *Self Organization in Non-equilibrium Systems: From Dissipative Structure to Order through Fluctuations* (Wiley, New York, 1977).

[3] N. Ghoniem and D. Walgraef, *Instabilities and Self Organization in Materials* (Oxford University Press, New York, 2008), Vol. 1.

[4] M. Cross and H. Greenside, *Pattern Formation and Dynamics in Non Equilibrium Systems* (Cambridge University Press, Cambridge, England, 2009).

[5] B. Bergersen and Z. Racz, Dynamical Generation of Long-Range Interactions: Random Levy Flights in Kinetic Ising and Spherical Models, Phys. Rev. Lett. **67**, 3047 (1991).

[6] M. Le Bellac, F. Mortessagne, and G. Batrouni, *Equilibrium and Non Equilibrium Statistical Thermodynamics* (Cambridge University Press, Cambridge, England, 2010).

[7] S. Dhal, A. Behera, and S. Chatterjee, Modification of ZnO nanowires induced by ion irradiation for device applications, J. At. Mol. Condens. Nanophys. **2**, 85 (2015).

[8] H. Bernas, J.-P. Attané, K.-H. Heinig, D. Halley, D. Ravelosona, A. Marty, P. Auric, C. Chappert, and Y. Samson, Ordering Intermetallic Alloys by Ion Irradiation: A Way to Tailor Magnetic Media, Phys. Rev. Lett. **91**, 077203 (2003).

[9] I. Beyerlein, A. Caro, M. Demkowicz, N. Mara, A. Misra, and B. Uberuaga, Radiation damage tolerant nanomaterials, Mater. Today **16**, 443 (2013).

[10] P. C. Hohenberg and B. I. Halperin, Theory of dynamic critical phenomena, Rev. Mod. Phys. **49**, 435 (1977).

[11] R. A. Enrique and P. Bellon, Compositional Patterning in Systems Driven by Competing Dynamics of Different Length Scale, Phys. Rev. Lett. **84**, 2885 (2000).

[12] D. Simeone, G. Demange, and L. Luneville, Disrupted coarsening in complex Cahn-Hilliard dynamics, Phys. Rev. E **88**, 032116 (2013).

[13] L. Luneville, K. Mallick, V. Pontikis, and D. Simeone, Patterning in systems driven by nonlocal external forces, Phys. Rev. E **94**, 052126 (2016).

[14] S. Chee, B. Stumphy, N. Vo, R. Averback, and P. Bellon, Dynamic self-organization in Cu alloys under ion irradiation, Acta Mater. **58**, 4088 (2010).

[15] P. Krasnochtchekov, R. S. Averback, and P. Bellon, Phase separation and dynamic patterning in $Cu_{1-x}Co_x$ films under ion irradiation, Phys. Rev. B **72**, 174102 (2005).

[16] G. Martin, Phase stability under irradiation: Ballistic effects, Phys. Rev. B **30**, 1424 (1984).

[17] V. Vaks and V. Kamyshenko, On the theory of open systems: Statistical thermodynamics and decomposition type phase transitions for the model of an alloy under irradiation, Phys. Lett. A **177**, 269 (1993).

[18] R. A. Enrique and P. Bellon, Nonequilibrium fluctuations, effective temperature, and effective interactions driven by irradiation of alloys, Phys. Rev. B **70**, 224106 (2004).

[19] R. A. Enrique and P. Bellon, Phase stability under irradiation in alloys with a positive heat of mixing: Effective thermodynamics description, Phys. Rev. B **60**, 14649 (1999).

[20] R. A. Enrique and P. Bellon, Self organized Cu-Ag nanocomposites synthesized by intermediate temperature ion-beam mixing, Appl. Phys. Lett. **78** (2001).

[21] A. Gras-Marti and P. Sigmund, Distortion of depth profiles during ion bombardment ii. mixing mechanisms, Nucl. Instrum. Methods Phys. Res., Sect. B **180**, 211 (1981).

[22] D. Simeone, G. Baldinozzi, D. Gosset, G. A. Demange, Y. Zhang, and L. Lunéville, An attempt to handle the nano-patterning of materials created under ion beam mixing, Mater. Res. Soc. Symp. Proc. **1514**, 49 (2013).

[23] K. Nordlund and R. S. Averback, Role of Self-Interstitial Atoms on the High Temperature Properties of Metals, Phys. Rev. Lett. **80**, 4201 (1998).

[24] T. Ohta and K. Kawasaki, Equilibrium morphology of block copolymer melts, Macromolecules **19**, 2621 (1986).

[25] D. Simeone, G. Thorogood, A. Forestier, P. Garcia, and L. Luneville, Radiation-induced micro-structures as ground states of a Swift-Hohenberg energy functional, J. Appl. Phys. **125**, 065103 (2019).

[26] G. Martin, Atomic mobility in Cahn's diffusion model, Phys. Rev. B **41**, 2279 (1990).

[27] M. Nonomura and T. Otha, Theory and simulation of mesoscopic morphological transitions, Physica (Amsterdam) **304A**, 77 (2002).

[28] M. Seul and D. Andelman, Domain shapes and patterns: The phenomenology of modulated phases, Science **267**, 476 (1995).

[29] K. R. Elder and M. Grant, Modeling elastic and plastic deformations in nonequilibrium processing using phase field crystals, Phys. Rev. E **70**, 051605 (2004).

[30] I. Jaatinen and T. Ala-Nissila, Extended phase diagram of the three-dimensional phase field crystal model, J. Phys. Condens. Matter **22**, 205402 (2010).

[31] A. Olemskoi and V. Klepikov, The theory of spatiotemporal pattern in nonequilibrium system, Phys. Rep. **338**, 571 (2000).

[32] D. Simeone, A. Millard, J. Ribis, C. Bacri, L. Largeau, P. Garcia, and L. Luneville (to be published).